Retinal Disease in Usher Syndrome III Caused by Mutations in the Clarin-1 Gene

Waldo Herrera,[1] Tomas S. Aleman,[1] Artur V. Cideciyan,[1] Alejandro J. Roman,[1] Eyal Banin,[2] Tamar Ben-Yosef,[3] Leigh M. Gardner,[1] Alexander Sumaroka,[1] Elizabeth A. M. Windsor,[1] Sharon B. Schwartz,[1] Edwin M. Stone,[4] Xue-Zhong Liu,[5] William J. Kimberling,[6] and Samuel G. Jacobson[1]

Purpose. To determine the retinal phenotype of Usher syndrome type III (USH3A) caused by clarin-1 (*CLRN1*) gene mutations in a non-Finnish population.

Methods. Patients with USH3A (n = 13; age range, 24–69) representing 11 different families were studied and the results compared with those from patients with USH2A (n = 24; age range, 17–66). The patients were evaluated by ocular examination, kinetic and static perimetry, near-infrared autofluorescence, and optical coherence tomography (OCT).

Results. Ten of 11 families had Ashkenazi Jewish origins and the N48K *CLRN1* mutation. Rod function was lost in the peripheral field in the first two decades of life, but central rod function could be retained for another decade. Peripheral cone function was detectable into the third decade of life. Central cone function had a slower decline that extended for decades. Photoreceptor layer loss and features of retinal remodeling were present in retinal regions with severe visual dysfunction, even at the youngest ages tested. Central retinal structure could be normal in younger patients but structural integrity was lost in older patients. RPE disease generally paralleled photoreceptor degeneration. Comparisons between USH3A and USH2A suggested a common rod and cone phenotype but a more accelerated time course of rod loss in USH3A.

Conclusions. USH3A and USH2A share patterns of rod and cone dysfunction and retinal structural abnormalities. Peripheral function measurements showed USH3A to be more rapidly progressive than USH2A. (*Invest Ophthalmol Vis Sci.* 2008;49:2651–2660) DOI:10.1167/iovs.07-1505

Major progress in understanding the molecular subcategories of Usher syndrome (USH) has occurred in recent years.[1] USH was first subcategorized in the clinic when two types of autosomal recessive deaf-blindness were defined: Patients with Usher I (USH1) had profound congenital sensorineural deafness, vestibular dysfunction, and retinitis pigmentosa (RP), and those with Usher II (USH2) had moderate congenital hearing impairment, normal vestibular function, and RP.[2,3] Evidence for a third USH subtype emerged as clinical observers noted progressive hearing loss in some patients with RP, and molecular scientists identified a chromosomal locus (USH3A, chromosome 3q25.1) and a causative gene (Clarin-1, *CLRN1*).[4–12] USH3A is now recognized as a separate entity with progressive hearing loss, variable vestibular abnormality, and RP. Although USH3A is relatively rare in most populations, it represents approximately 40% of USH cases in Finland[8,13,14] and in Ashkenazi Jews.[10,11,15]

USH3A poses an especially difficult diagnostic challenge considering there is progressive hearing impairment and progressive retinal degeneration, both with variable onset.[16,17] Patients at some ages can present as nonsyndromic RP with little or no hearing loss, whereas many USH3A patients have hearing loss and masquerade as other USH subtypes. The ocular phenotype of USH3 has been described and compared with USH1 and USH2 in premolecular studies of the Finnish population.[18] A reanalysis of these data, but with molecular clarification as USH3A-*CLRN1*, has been reported recently.[19]

To understand details of the retinal disease expression in USH3A, we explored a non-Finnish USH3A-*CLRN1* patient population by determining rod- and cone-mediated visual function and performing en face and cross-sectional retinal imaging. Function and structure in USH3A were compared with results in USH2A.

Methods

Human Subjects

Thirteen patients (age range, 24–69 years) with USH3A-*CLRN1* mutations (Table 1) and 24 patients (age range, 17–66 years) with USH2A (Table 2) were included. Patients with USH2A had the clinical diagnosis of either USH2 (n = 15; 14 reported[20]) or nonsyndromic RP (n = 9). All patients had a complete eye examination. Informed consent was obtained; procedures adhered to the Declaration of Helsinki and had institutional review board approval.

Visual Function

Kinetic and static threshold chromatic perimetry were performed and analyzed as published.[21–23] Static thresholds were determined with 1.7° diameter, 200-ms duration stimuli under dark-adapted (500-,

From the [1]Scheie Eye Institute, Department of Ophthalmology, University of Pennsylvania, Philadelphia, Pennsylvania; the [2]Department of Ophthalmology, Hadassah-Hebrew University Medical Center, Jerusalem, Israel; the [3]Department of Genetics and the Rappaport Family Institute for Research in the Medical Sciences, Faculty of Medicine, Technion-Israel Institute of Technology, Haifa, Israel; the [4]Howard Hughes Medical Institute and Department of Ophthalmology, University of Iowa Carver College of Medicine, Iowa City, Iowa; the [5]Department of Otolaryngology, University of Miami, Miami, Florida; and the [6]Usher Syndrome Center, Boys Town National Research Hospital, Omaha, Nebraska.

Supported by grants from the Foundation Fighting Blindness, National Neurovision Research Institute, Hope for Vision, Macula Vision Research Foundation, Macular Disease Foundation, The Chatlos Foundation, Research to Prevent Blindness, the Ruth and Milton Steinbach Fund, and the Alcon Research Institute.

Submitted for publication November 22, 2007; revised January 24, 2008; accepted April 14, 2008.

Disclosure: **W. Herrera**, None; **T.S. Aleman**, None; **A.V. Cideciyan**, None; **A.J. Roman**, None; **E. Banin**, None; **T. Ben-Yosef**, None; **L.M. Gardner**, None; **A. Sumaroka**, None; **E.A.M. Windsor**, None; **S.B. Schwartz**, None; **E.M. Stone**, None; **X.-Z. Liu**, None; **W.J. Kimberling**, None; **S.G. Jacobson**, None

The publication costs of this article were defrayed in part by page charge payment. This article must therefore be marked "*advertisement*" in accordance with 18 U.S.C. §1734 solely to indicate this fact.

Corresponding author: Samuel G. Jacobson, Scheie Eye Institute, University of Pennsylvania, 51 N. 39th Street, Philadelphia, PA 19104; jacobsos@mail.med.upenn.edu.

TABLE 1. Clinical and Molecular Characteristics of the USH3A Patients

Family (Mutation), Patient	Age at First Visit (y)/Sex	Eye	Visual Acuity*	Refraction	Kinetic Visual Field Extent (V-4e/I-4e)†	Hearing Impairment‡
Family 1 (N48K/N48K)						
P1	24/M	RE	20/100§	−1.50 +1.25 × 015	6/1	Moderate
		LE	20/50§	−1.00 +0.75 × 074	7/1	
Family 2 (N48K/N48K)						
P1	28/F	RE	20/25	−3.50 +0.75 × 084	12/<1	Moderate
		LE	20/25§	−3.25 +0.75 × 121	13/<1	
Family 3 (N48K/N48K)						
P1	29/F	RE	20/20‖	−1.50 +1.50 × 180	83/1	None
		LE	20/20‖	−1.50 +1.50 × 180	83/<1	
Family 4 (N48K/N48K)¶						
P1	30/F	RE	20/50§#	+0.75 sph	NA	Moderate
		LE	20/125§#	+0.75 sph		
Family 5 (N48K/N48K)						
P1	32/F	RE	20/25	Plano**	2/<1**	Moderate
		LE	20/32	−0.75 −0.50 × 70**	2/<1**	
Family 6 (N48K/N48K)						
P1	36/F	RE	20/40#	−2.25 +0.50 × 142	20/ND	Severe
		LE	20/160‖#	−2.00 +0.25 × 052	22/ND	
Family 7 (N48K/N48K)						
P1	38/M	RE	20/400#	−5.00 +2.50 × 095	3/ND	Mild
		LE	20/80#	−5.00 +2.50 × 085	3/ND	
P2	45/M	RE	20/63‖#	−3.75 +0.75 × 115	1/<1	Moderate
		LE	20/50‖#	−4.75 +1.25 × 140	1/<1	
Family 8 (N48K/L150P)††						
P1	39/F	RE	20/63#	+2.75 +0.75 × 040	3/<1	Severe
		LE	20/250§	+3.00 +0.50 × 135	3/ND	
Family 9 (N48K)‡‡						
P1	63/F	RE	20/800#	+2.50 sph	2/ND	Severe
		LE	20/800#	+3.00 sph	1/ND	
Family 10 (N48K)‡‡						
P1	69/F	RE	20/500	Aphakia	ND/ND	Severe
		LE	20/500	Aphakia	<1/ND	
Family 11 (D55fs)†††‡‡						
P1	37/F	RE	20/25	−1.00 +2.50 × 015	3/1	Severe
		LE	20/25	−1.00 +2.20 × 166	3/<1	
P2	38/M	RE	20/50	Pseudophakia	1/<1	Severe
		LE	20/63#	Plano +1.00 × 150	2/<1	

ND, not detectable; NA, not available.
* Best corrected visual acuity.
† Expressed as a percentage of the normal mean for the V-4e or I-4e target; 2 SD below the mean is 90%.
‡ By clinical history; patients reported progressive hearing loss.
§ Cystoid macular edema.
‖ Epiretinal membrane.
¶ Genotype and some clinical characteristics previously reported.[15]
# Minimal posterior subcapsular cataract.
** Refraction and kinetic visual field extent from visit at 38 years of age.
†† Family's genotype previously reported.[11]
‡‡ Only one allele identified.

650-nm stimuli) and light-adapted (600 nm) conditions. A full-field test of 72 loci on a 12° grid and a horizontal profile across the fovea (extending 60° at 2° intervals) were used. Photoreceptor mediation was based on the sensitivity difference in the responses to 500 and 650 nm stimuli.[21,23] Rod sensitivity loss (500 nm, dark adapted) at each test locus was determined by comparison with normal mean sensitivity at that location. Loci were considered to have no measurable rod sensitivity if loss was >30 dB.[23] Cone-mediated function from dark-adapted perimetry was compared with normal results measured during the cone plateau of dark adaptation. The extent of the static field was defined as the number of locations mediated by rods or cones and expressed as a percentage of the total number of loci tested (12° grid; 70 extrafoveal loci for rods; 71 for cones),[21] or as the average of an abbreviated set of central loci (16°) from the dark-adapted horizontal profile.[23] Mean rod sensitivity was defined as the average of sensitivities to 500 nm from all loci with rod-mediated detection; mean cone sensitivity was the average of sensitivities detecting the 600-nm stimulus. Electroretinograms (ERGs) were performed with a standard protocol.[22,24]

En Face Imaging with Scanning Laser Ophthalmoscope (SLO)

Near-infrared (NIR) light was used to perform en face imaging with a confocal SLO without subjecting the diseased retina to undue light exposure. Reflectivity distribution of retinal and subretinal features was imaged with 820-nm NIR light. The health of the RPE was estimated with 790-nm NIR excitation light with a recently described reduced-illuminance autofluorescence imaging (RAFI) technique.[25] The NIR-RAFI signal is believed to be dominated by the melanolipofuscin in RPE and melanin in the RPE and choroid.[25–28] Disease-related changes in RPE melanin/melanolipofuscin content results in spatial variation of the NIR-RAFI signal intensity, appearance, or both. In most cases, HRA2 (Heidelberg Engineering GmbH, Heidelberg, Germany) was used for imaging in the high-resolution mode; 30° × 30° of retina

TABLE 2. Clinical and Molecular Characteristics of the USH2A Patients

Family (Mutation), Patient	Age at First Visit (y)/ Sex	Eye	Visual Acuity*	Refraction	Kinetic Visual Field Extent (V-4e/I-4e)†	Electroretinograms: Amplitude‡ Rod b-wave	Electroretinograms: Amplitude‡ Cone Flicker	Electroretinograms: Cone Flicker Timing
Family 1 (E767fs/P3272L)								
P1	22/F	RE	20/32	−8.00 +2.00 × 096	66/2	ND	4	Delayed
		LE	20/25	−8.00 +2.00 × 081	60/2			
Families 2–11 (data published[20])								
Family 12 (C759F/W3955X)								
P1	24/M	RE	20/20	−0.75 +0.75 × 098	100/2	14	27	Delayed
		LE	20/20	−0.75 +1.00 × 091	100/2			
Family 13 (E767fs)§								
P1	26/M	RE	20/20‖	−0.50 sph	91/16	13	9	Delayed
		LE	20/20‖	−1.25 +0.50 × 070	86/14			
Family 14 (E767fs)§								
P1	27/F	RE	20/20	−0.50 +2.50 × 020	100/39	23	13	Delayed
		LE	20/20	−1.00 +2.50 × 159	100/41			
Family 15 (C759F)§								
P1	32/F	RE	20/25	Plano	50/<1	ND	6	Delayed
		LE	20/32	Plano	70/<1			
Family 16 (C759F/V218E)								
P1	43/F	RE	20/20	−1.00 +1.00 × 105	87/23	18	50	Delayed
		LE	20/20	−1.00 +1.00 × 090	90/51			
Family 17 (E767fs)§								
P1	47/M	RE	20/20‖	−2.75 +1.75 × 020	40/<1	ND	4	Delayed
		LE	20/20‖	−3.25 +2.00 × 070	40/1			
Family 18 (C759F)§								
P1	58/M	RE	20/25	Pseudophakia	<1/<1	NP	NP	NP
		LE	20/32	Pseudophakia	<1/<1			
Family 19 (C759F)§								
P1	61/M	RE	20/25	Aphakia	<1/<1	ND	ND	ND
		LE	20/32	Pseudophakia	<1/<1			
Family 20 (E767fs/C759F)								
P1	66/M	RE	20/50‖	−1.25 sph	6/ND	ND	3	Delayed
		LE	20/630‖	−1.50 +0.50 × 120	2/ND			

N, normal; NP, not performed; ND, not detectable.

* Best corrected visual acuity.

† Expressed as a percentage of the normal mean for the V-4e or I-4e target; 2 SD below the mean is 90%.

‡ Expressed as a percentage of the normal mean amplitude (rod, 292 μV; cone flicker, 172 μV); 2 SD below normal is 67% for rod b-wave and 60% for cone flicker.

§ One allele identified only.

‖ Minimal posterior subcapsular cataract.

is sampled onto a 1536 × 1536-pixel image, and 25-frame video sequences were obtained at the rate of 4.7 Hz. Detector sensitivity was set to 95% for NIR-RAFI. Images were exported from the manufacturer's software and analyzed as described.[25,28] NIR-RAFI signal intensity was estimated along a 30-pixel-high (176 μm) horizontal profile passing through the fovea. In one patient with USH2A (family [F]3, patient [P]1), images were obtained with HRA1, and the resulting intensities were converted to HRA2-equivalent values.

Optical Coherence Tomography (OCT)

Cross-sectional images of the retina were obtained with commercially available OCT instruments (OCT1 and OCT3; Carl Zeiss Meditec, Dublin, CA). In all subjects, overlapping 4.5-mm-length scans were used to study a 9-mm extent along the horizontal meridian through the fovea. Each scan, formed by a series of longitudinal reflectivity profiles (LRPs), was analyzed with custom-developed software (MatLab ver. 6.5; The MathWorks, Natick, MA) and published methods.[29,30] Overall retinal thickness, nuclear layers, and an inner retinal thickness parameter were defined.[29–32]

For topographic analysis, the precise location and orientation of each scan relative to retinal features (blood vessels, optic nerve head) were determined using video images of the fundus. LRPs were allotted to regularly spaced bins in a rectangular coordinate system centered at the fovea, and the waveforms in each bin were aligned and averaged. For two-dimensional maps, 0.3 × 0.3-mm^2 bins were used for sampling, whereas 0.15 × 0.15-mm^2 bins were used for analysis along the horizontal and vertical meridians. The overall retinal, outer nuclear layer (ONL), and inner retinal thickness were measured. Missing data were interpolated bilinearly. Thicknesses were mapped to a pseudocolor scale, and fundus landmarks were overlaid for reference.[32,33]

RESULTS

Molecular and Clinical Features of USH3A

Patients with USH3A from families 1 to 7 were homozygous for the N48K *CLRN1* mutation, the prevalent result in Ashkenazi Jews.[10,11,15] F8,P1 was a compound heterozygote for the N48K and L150P mutations.[11] Patients from families 9 and 10 also carried the N48K mutation, but a second allele has not been identified. Families 1 to 10 had Ashkenazi Jewish origins. Family 11 was of Dutch origin and a single allele, D55fs (165delC), was identified.[11,34]

Hearing impairment was reported by all patients except F3,P1, who had a normal audiogram. Childhood-onset hearing disturbances were described by most patients; only F7,P1 recalled an adult onset (Table 1). Audiometry results, available in six of these patients, indicated bilateral moderate to severe sensorineural hearing loss.[34] Serial audiometry in members of family 11 confirmed the progressive nature of the hearing loss.[34]

Patients with USH3 have been reported to show hyperopic refractive errors with astigmatism.[18,19] The refractive error (spherical equivalent; both eyes averaged) of patients with USH3A in the present study ranged from +3.50 to −3.75 D (mean ± SD = −0.53 ± 2.32; n = 12 patients), and 10 of 12 patients had astigmatism in at least one eye (Table 1). There was also a range of refractive errors in patients with USH2A (+0.50 to −7.00 D; mean ± SD = −1.78 ± 1.96; n = 19) and most (14/19) had astigmatism (Table 2). A comparison of spherical equivalents in the two molecular groups showed no significant difference (unpaired t-test, P = 0.12), and the ranges of astigmatic errors were overlapping.

Kinetic visual fields in two USH3A N48K homozygotes illustrated that there can be different degrees of peripheral visual abnormality in patients of similar age. F3,P1 at age 29 had a full kinetic field to the large (V-4e) target but a limited central island to the small (I-4e) target. F1,P1 at age 24 had a central island separated from a temporal peripheral island by a complete annular midperipheral scotoma (Fig. 1A). Kinetic field extent (V-4e) was plotted against age in the patients with USH3A. Data from the patients with USH2A are also shown (Fig. 1B). The three patients with USH3A in the third decade of life had different extents of kinetic fields. Eight (89%) of nine patients with USH3A over age 30 had fields reduced to a central island only; the exception, F6,P1 at age 36, retained peripheral islands. Among 13 patients with USH2A older than 30 years, 5 (38%) had only central islands remaining; the others retained peripheral islands.

Longitudinal data for kinetic fields in most of our patients with USH3A were not available except as medical records or at stages when only a central island remained. We asked whether our cross-sectional USH3A data fell within the range of the progressive field loss in patients with USH2A, for whom we had longitudinal data. Comparative summary statistics for the patients with USH2A were derived from serial kinetic fields (Fig. 1B, symbols connected by black lines) from nine patients over an average follow-up period of 11.5 years (range, 3–20 years). The mean (SE) annual exponential rate of decline for USH2A was 10.7% (3.4%). The corresponding critical age at the lower limit of normal area (90%) was 25.4 years and the half-life of field loss was 6.5 years (Fig. 1B, thick gray line).

An anecdotal datum of interest was in USH3A patient F2,P1. When the patient was 12 years of age, a kinetic field (from medical records) showed midperipheral absolute scotomas but full peripheral extent. We quantified this field to be 80% of normal (Fig. 1B, small circle). At age 28 (Table 1), the field had become reduced to a central island separated from a temporal island, corresponding to only 12% of normal (Fig. 1B). Assuming the loss of visual field extent over time follows an exponential decline,[35–40] the data from F2,P1 would correspond to an annual exponential rate of decline of 12.8%. The critical age would be estimated as 12.3 years for this patient with USH3A. Kinetic perimetry results suggest that most USH3A data fall either on or near the most rapidly progressive field loss expected in USH2A (Fig. 1B, thin gray lines).

To compare foveal function in USH3A with that in USH2A, best corrected visual acuity (BCVA) was analyzed (Fig. 1C). Mean (SE) BCVA in USH3A in the first three decades of life (n = 7; better-seeing eye) was 0.07 (0.04) logMAR compared with 0.06 (0.03) logMAR in USH2A (n = 12); this difference was not

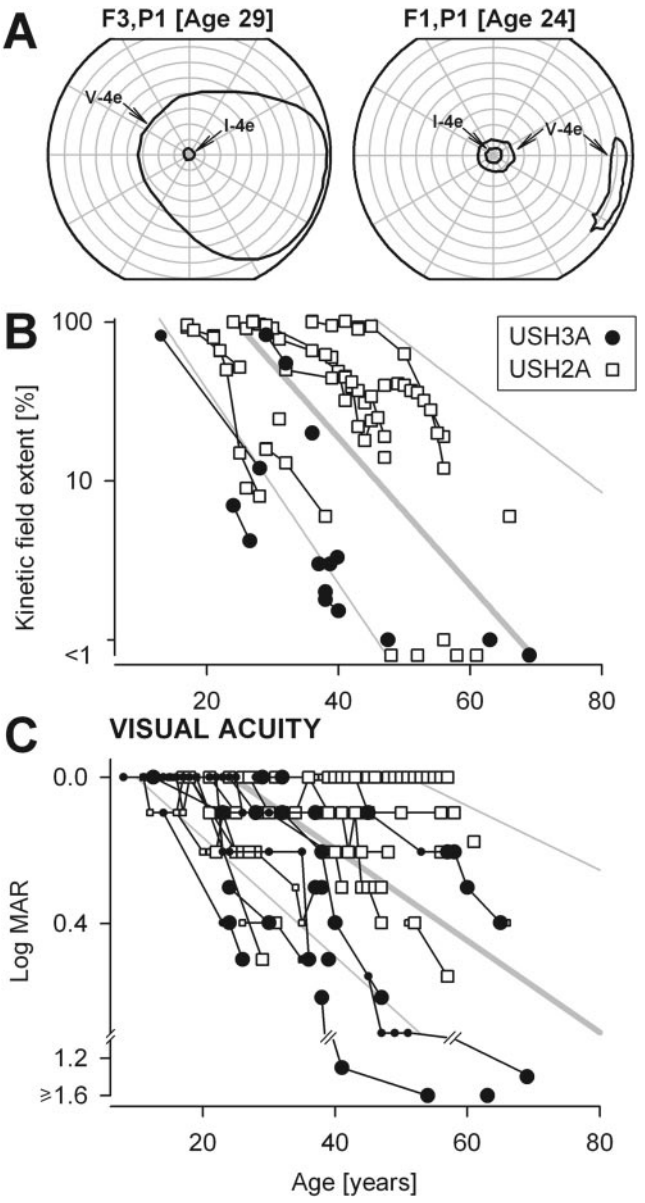

FIGURE 1. Kinetic visual fields and visual acuity in USH3A compared with those in USH2A. (**A**) Kinetic perimetry in two patients with USH3A of comparable age. (**B**) Extent of the kinetic visual field (V-4e target) expressed as a percentage of normal mean and plotted as a function of age in patients with USH3A compared with those with USH2A. (**C**) BCVA as a function of age in USH3A and USH2A. (**B**, **C**). Serial measurements are connected by *solid lines*; *smaller symbols* represent data from medical records. *Gray thick line:* mean exponential rate of decline of parameter with age (±SE, *thin gray lines*) derived from regressions fit to individual serial measurements in patients with USH2A.

significant (P = 0.80). However, there was a tendency for greater persistence of BCVA with age in USH2A compared to USH3A. At ages greater than 30, mean BCVA of 0.60 (0.21) logMAR in USH3A (n = 6) was significantly worse than 0.16 (0.04) logMAR in USH2A (n = 12; P = 0.01). Taking together our longitudinal data (Fig. 1C; large circles) and those from patient records (small circles), the annual exponential rate of decline of BCVA in USH3A was 7.2% (0.03 logMAR/year; n = 12). The rate in USH2A was 2.9% (0.01 logMAR/year; n = 18), and the difference from that in USH3A was not significant (P = 0.32). These estimates of BCVA progression rates were inter-

mediate to those previously published in serial studies of RP[35,38,41] and similar to the rates estimated from cross-sectional studies of patients with USH1 or USH2.[42–45]

Rod- and Cone-Mediated Visual Function

Rod-mediated function in the peripheral field was not detectable in F3,P1 and F1,P1, the youngest of the patients with USH3A tested with dark-adapted perimetry in this study ($n = 11$). Peripheral cone function was present in F3,P1, but F1,P1 had cone sensitivity only at and near fixation (Fig. 2A). Patients with USH3A or USH2A were compared for rod- and cone-mediated peripheral function, as quantified with dark- and light-adapted perimetry throughout the visual field.[21] The area of visual field representing each photoreceptor type was defined as the number of loci mediated by rods (with <3.0 log units of sensitivity loss) or cones and expressed as a percentage of the total number of loci analyzed. Rod- and cone-mediated areas were plotted against patient age (Fig. 2B). Patients with USH3A had essentially no measurable rod area (except F3,P1) and this is consistent with nondetectable rod ERGs in these patients (data not shown). Six patients with USH2A, ranging in age from 17 to 43, retained substantial areas with rod function (24%–91% of loci). Mean rod sensitivity loss in these patients ranged from 1.1 to 2.3 log units. Most of these patients (5/6) had detectable rod ERG b-waves (Table 2).[20] A mean (SE) annual exponential rate of rod area decline of 18.8% (2.4%) was estimated from longitudinal data available in three patients with USH2A. Only two patients with USH3A (2/11; 18%) had a substantial peripheral cone area (≥10% of loci; Fig. 2B). F3,P1, age 29, had mean cone sensitivity loss of 1.1 log units; F6,P1, age 36, had a mean loss of 1.4 log units. By comparison, more than half of the patients with USH2A (16/24; 66%; age range, 17–47) showed considerable peripheral cone function. Mean cone sensitivity losses in these patients ranged from 0.5 to 1.5 log units. Longitudinal cone area data available in eight patients

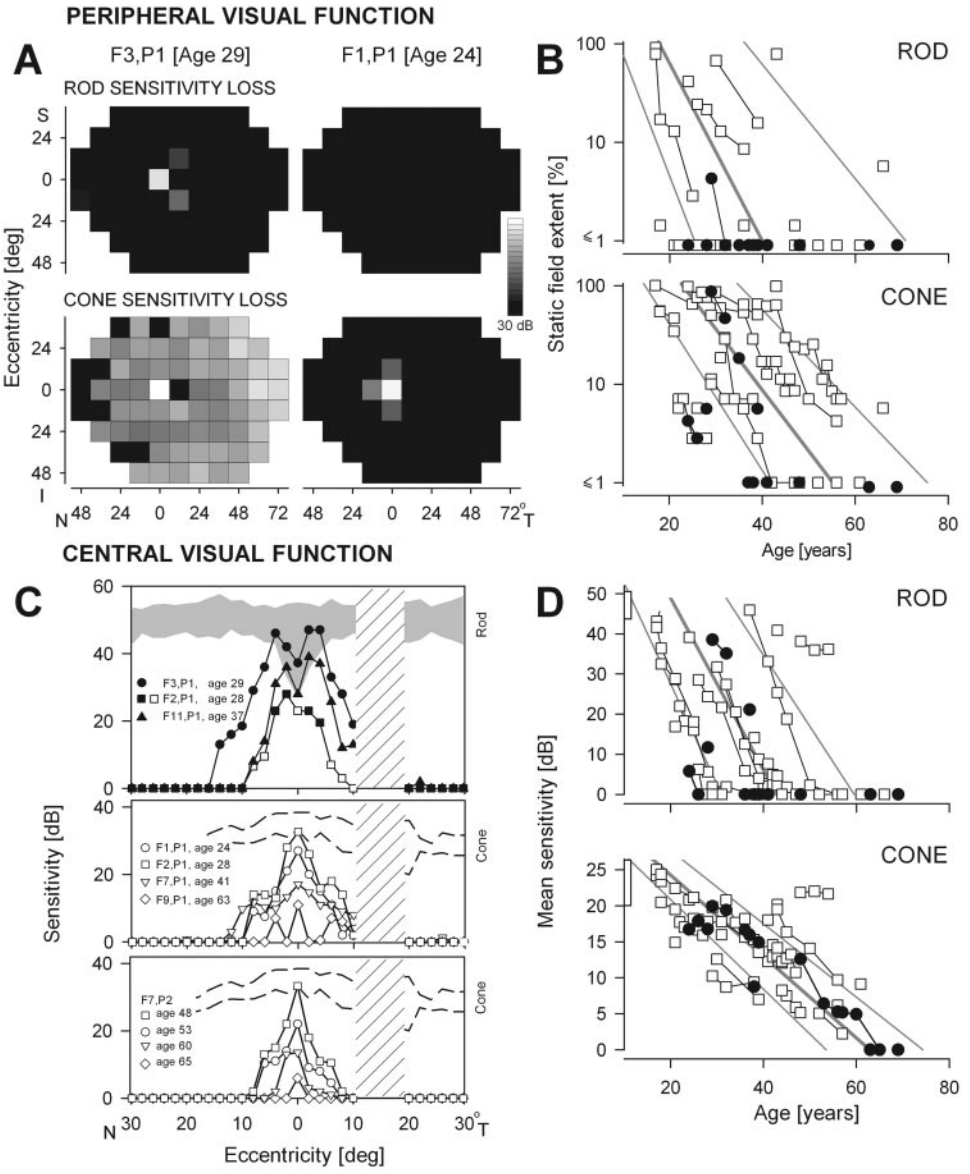

FIGURE 2. Rod- and cone-mediated peripheral and central visual function in USH3A compared with USH2A. (**A**) Static perimetry of two patients with USH3A (right eyes) displayed as grayscale maps of rod (dark-adapted, *top*) and cone (light-adapted, *bottom*) sensitivity loss. Scale has 16 levels of *gray*, representing 0- to 30-dB losses. The physiological blind spot is shown as a *black square* at 12° in the temporal field. (**B**) The extent of static visual field perceived by rods (*top*) or cones (*bottom*) expressed as a percentage of sampled points and plotted as a function of age for USH3A (*circles*) and USH2A (*squares*). (**C**) Rod- and cone-mediated sensitivity profiles across the central 60° in USH3A. *Top:* dark-adapted profiles (500 nm) in three patients illustrating rod abnormalities. *Shaded area*: normal range (mean ± 2 SD; $n = 21$; age range, 15–42) for rod-mediated sensitivity to this stimulus. *Middle* and *bottom:* dark-adapted profiles (650 nm) illustrating increasing cone-mediated disease with age as cross-sectional data (*middle*) in four patients or as longitudinal data in one patient (*bottom*) over a 17-year interval. *Dashed lines*: normal limits (mean ± 2 SD; $n = 5$; age range, 26–54) for the 650-nm stimulus at the cone plateau. *Filled symbols*: rod-mediated sensitivities; *open symbols*: cone-mediated sensitivities. *Hatched area*: physiological blind spot. (**D**) Mean sensitivities for rods (*top*, 500 nm, dark-adapted) or cones (*bottom*, 600 nm, light-adapted) from central field profiles (±8°) in patients plotted as a function of age for USH3A (*circles*) and USH2A (*squares*). Bars on vertical axes define normal sensitivity (mean ± 2 SD). (**B**, **D**) Serial measurements (connected by *lines*) available in patients with USH2A are individually fit with exponential decay functions and parameters derived. *Gray thick line*: mean exponential rate of decline of static field (extent or sensitivity) with age derived from the average (±SE, *thin gray lines*) of the regressions fit to individual serial measurements in patients with USH2A. Visual fields indicate N, nasal; T, temporal; I, inferior; and S, superior.

with USH2A allowed estimation of the mean annual exponential rate of cone area decline as 13.3% (2.8%; Fig. 2B).

Central rod- and cone-mediated visual function was also studied. Rod-mediated sensitivity in the central field was detected in only four patients with USH3A (Fig. 2C, top). F3,P1, at age 29 years, had normal rod sensitivity within the central 8°, but this became diminished with increasing eccentricity. Detectable but abnormal rod-mediated function was found in F2,P1 at age 28 and in F11,P1 at age 37; there were only two rod-mediated loci near fixation in a fourth patient (F1,P1; data not shown). Central cone-mediated function was present in all patients with USH3A tested, and the results tended to be more abnormal in older patients (Fig. 2C, middle). Longitudinal measurements of central function in F7,P2 over a 17-year interval show how the cone-mediated island of this patient at age 48 diminished in sensitivity and extent with disease progression (Fig. 2C, bottom). These cross-sectional and limited longitudinal data suggest a disease sequence in the central retina of USH3A: normal rod function proceeds to abnormal rod function and subsequently to cone-only function, which becomes reduced with time.[20]

We asked whether patients with USH3A differed in residual central function from those with USH2A. Dark- and light-adapted perimetric profiles were used to calculate mean sensitivity[23] and results plotted against age (Fig. 2D). Only four patients with USH3A (4/11; 36%) had detectable rod-mediated sensitivity, and these patients were 24, 28, 29, and 37 years of age. The remaining patients had no measurable rod function in the central island. More than half of the patients with USH2A (16/23; 69%) had rod-mediated central islands; the age range of these patients was 17 to 47 years (Fig. 2D, top).

Cone-mediated function was quantified using light-adapted static perimetry in the central field (Fig. 2D, lower). With the exception of the two oldest patients (F9,P1; F10,P1), all patients with USH3A tested had measurable but abnormal central islands of cone function. All patients with USH2A also had measurable central cone function, but many were within normal limits (7/22, 32%). From the cross-sectional data, an average rate of loss of 0.29 dB per year was calculated for patients with USH3A; a similar rate, 0.27 dB per year, was present in USH2A. Longitudinal central data for USH2A permitted comparison of the declines with age of rod- versus cone-mediated data. The rate of decline for rods was 2.14 dB per year, whereas that for cones was 0.57 dB per year, and these rates were significantly different ($P < 0.0001$).

En Face and Cross-sectional Retinal Imaging

NIR-RAFI was used to estimate RPE melanin integrity in patients with USH3A (Fig. 3A), and the results were compared with images from patients with USH2A (Fig. 3B). Normal NIR-RAFI shows a circular region (~2-mm diameter) of higher brightness centered at the fovea, surrounded by a lower brightness signal across most of the retina; retinal blood vessels and the optic nerve head appear darker (Fig. 3, bottom right). USH3A patient F3,P1 (age 33) showed NIR-RAFI topography with a central elliptical region of relatively high autofluorescence signal and a transition to lower signal more peripherally (Fig. 3A). This pattern has been observed in patients with RP of unknown genotype and in patients with LCA caused by *CEP290* mutations and corresponds to the central retinal region of relative preservation.[28] NIR-RAFI topography in USH3A patient F2,P1 (age 28) showed central annuli of alternating intensity. Notable was the parafoveal ring of higher autofluorescence and a transition from a relatively homogenous region to more heterogeneity at an eccentricity of ~2.5 mm. F6,P1 (age 36) had only a small (~1-mm diameter), irregular central island of relatively high signal surrounded by a parafoveal ring of negligible signal surrounded by a relatively low signal. There was an approximately circular transition (at ~2.5 mm eccentricity) from a homogenous-appearing signal to a distinctly choroidal-appearing signal, suggesting a major loss of RPE melanin. F8,P1 (data not shown) had a pattern of results similar to those of F6,P1. Patients with USH2A ($n = 4$; age range, 22–57 years) were also studied. F3,P1 and F17,P1 differed in age by approximately 35 years but showed a similar pattern of NIR-RAFI topography with a central high autofluorescence signal and an elliptical boundary transition to a low signal more peripherally. NIR-RAFI topography in USH2A patients F4,P1 (age 39) and F15,P1 (age 48) were similar in intensity and pattern to USH3A patients F2,P1 and F6,P1, respectively, suggesting an overlap of RPE disease phenotype at some stages of USH2A and USH3A disease. Quantitation of the NIR-RAFI intensity along the horizontal meridian shows greater retention of melanin fluorescence and RPE health in central regions of both USH3A and USH2A patients.

Topographical maps across an expanse of central retina illustrate ONL and inner retinal thickness in a normal subject (Fig. 4A) and two patients with USH3A (Figs. 4B, 4C). In the normal retina, the ONL peaked centrally and declined with distance from the fovea; parafoveal thinning was more gradual in the superior retina. F2,P1 (age 28) retained a central island of ONL with a small central peak that was normal in thickness (Fig. 4B, inset). This island was surrounded by an undetectable photoreceptor layer and then a detectable but abnormally reduced ONL near the vascular arcades. F6,P1 (age 36) showed a small central peak of reduced ONL thickness surrounded by regions of nonmeasurable or minimally detectable ONL (Fig. 4C). Inner retinal thickness topography in the normal retina showed a foveal depression surrounded by an annulus of increased thickness and also a crescent of greater thickness extending toward the optic nerve. The patients with USH3A showed inner retinal thickness that was greater than normal, except at the fovea and surrounding the optic nerve (Fig. 4B, 4C). The 36-year-old patient showed greater thickness of the inner retina than did the 28-year-old patient.

Cross-sectional OCT images through the central retina are shown for a normal subject and patients with USH3A or USH2A in their third decade of life (Fig. 4D). The normal retina had a foveal depression and the surrounding retina was laminated with low-reflectivity cellular layers and intervening hyperreflective synaptic laminae. The patient with USH3A showed a foveal depression with normal-appearing foveal ONL thickness. The ONL diminished in thickness with eccentricity from the fovea and became abnormally thinned. A patient with USH2A showed a similar pattern of preserved central structure but increasing abnormality with eccentricity. Colocalized central rod- and cone-mediated function (above the images) indicates that at these disease stages, rod and cone function was preserved to an eccentricity of approximately 3 mm from the fovea. At greater eccentricities, cone sensitivity was reduced, and rod function was not detectable. The overall retina, ONL, and inner retina in 10 patients with USH3A and 11 patients with USH2A are quantified for thickness across the horizontal meridian (Fig. 4E). Data are plotted in relation to normal limits (mean ± 2SD). Patients with USH3A are identified by individual symbols, and both groups share color-coding for age (<30 years, yellow symbols; ≥30, red). The groups seem to follow the same general trends, with retinal thickness decreasing at increased ages. Greater preservation of thickness in the more central retina was common, but loss of foveal thickness did occur. ONL measurements indicated that younger patients in each group could have a normal ONL thickness at the fovea. One young patient with USH2A (F2,P4; Table 2; see also Ref. 20) had a normal ONL across the central region examined; but others had an ONL measurable only within the central 3 mm.

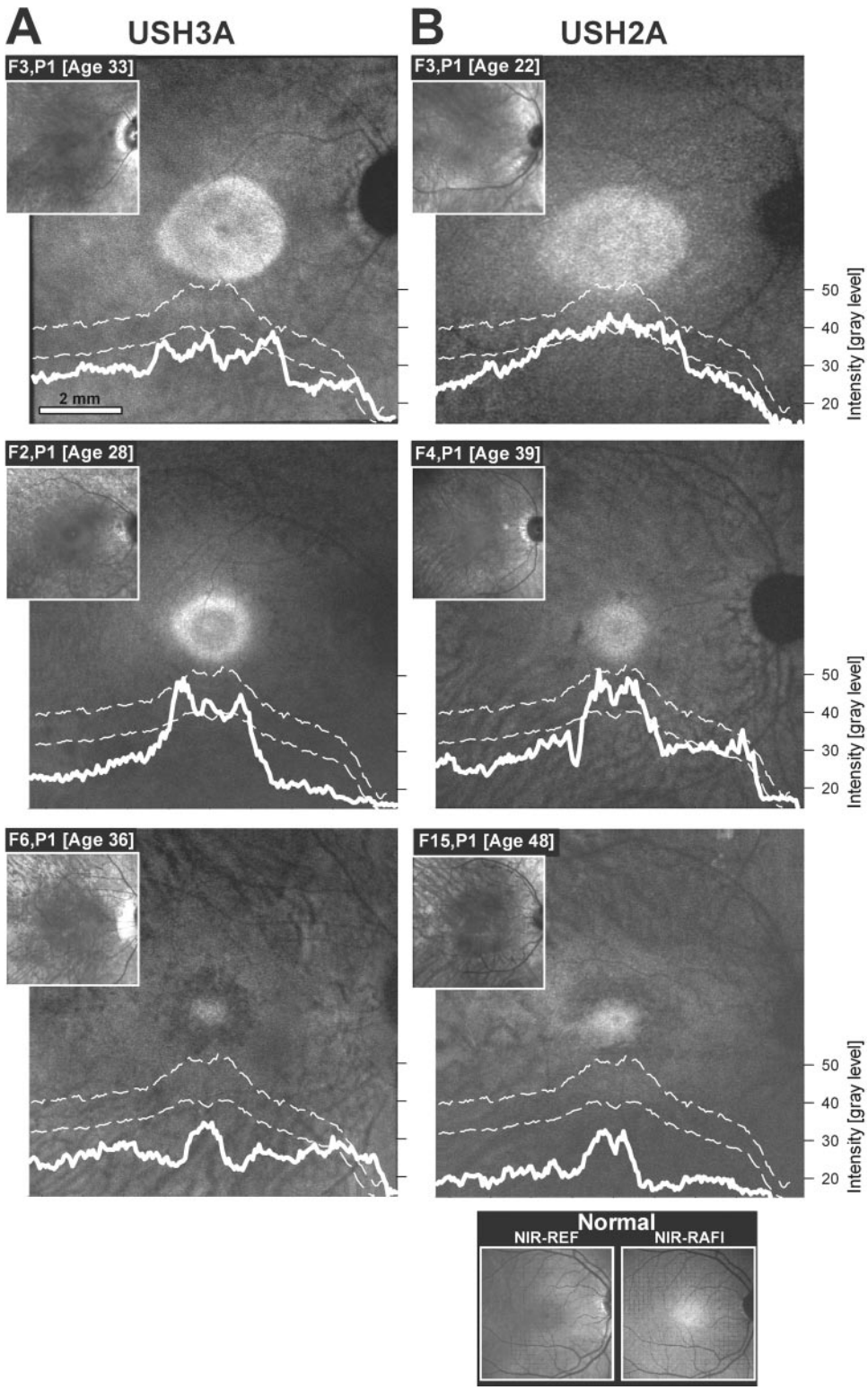

FIGURE 3. NIR-RAFIs of RPE health in three patients with USH3A (**A**) are compared with those in three patients with USH2A (**B**). *Insets*: the NIR reflectance (NIR-REF) image of each subject. All images are shown as equivalent right eyes and are individually contrast stretched for better visibility of features. Overlays show NIR-RAFI intensity along the horizontal profile crossing the fovea (*thick white lines*) compared with the confidence interval (±2 SE, *thin dashed lines*) of the normal mean derived from 19 subjects (age range, 7–63 years). *Bottom right*: representative normal NIR-REF and NIR-RAFI images shown for comparison.

Increasing age tended to be associated with the loss of ONL, leading to small central islands of substantially reduced ONL. Inner retinal thickness is normally at a minimum in the fovea. Parafoveal thickening, a feature of normal retina, was also present in USH3A and USH2A. At eccentricities beyond ~2 to 3 mm eccentric to the fovea, some patients showed normal inner retinal thickness, whereas the thickness in others was hypernormal. Such a hyperthick paracentral inner retina has been documented in other retinal degenerations.[30–32,46,47]

DISCUSSION

Human USH genetics has become increasingly complex, with many molecular subtypes of the three clinical types.[17] The exact retinal disease mechanisms in these genetically heterogeneous USH subtypes are not understood. It has been proposed that there may be a common pathogenesis due to an interactive network of USH-associated molecules.[1,48–51] An emerging concept is that these proteins, which belong to

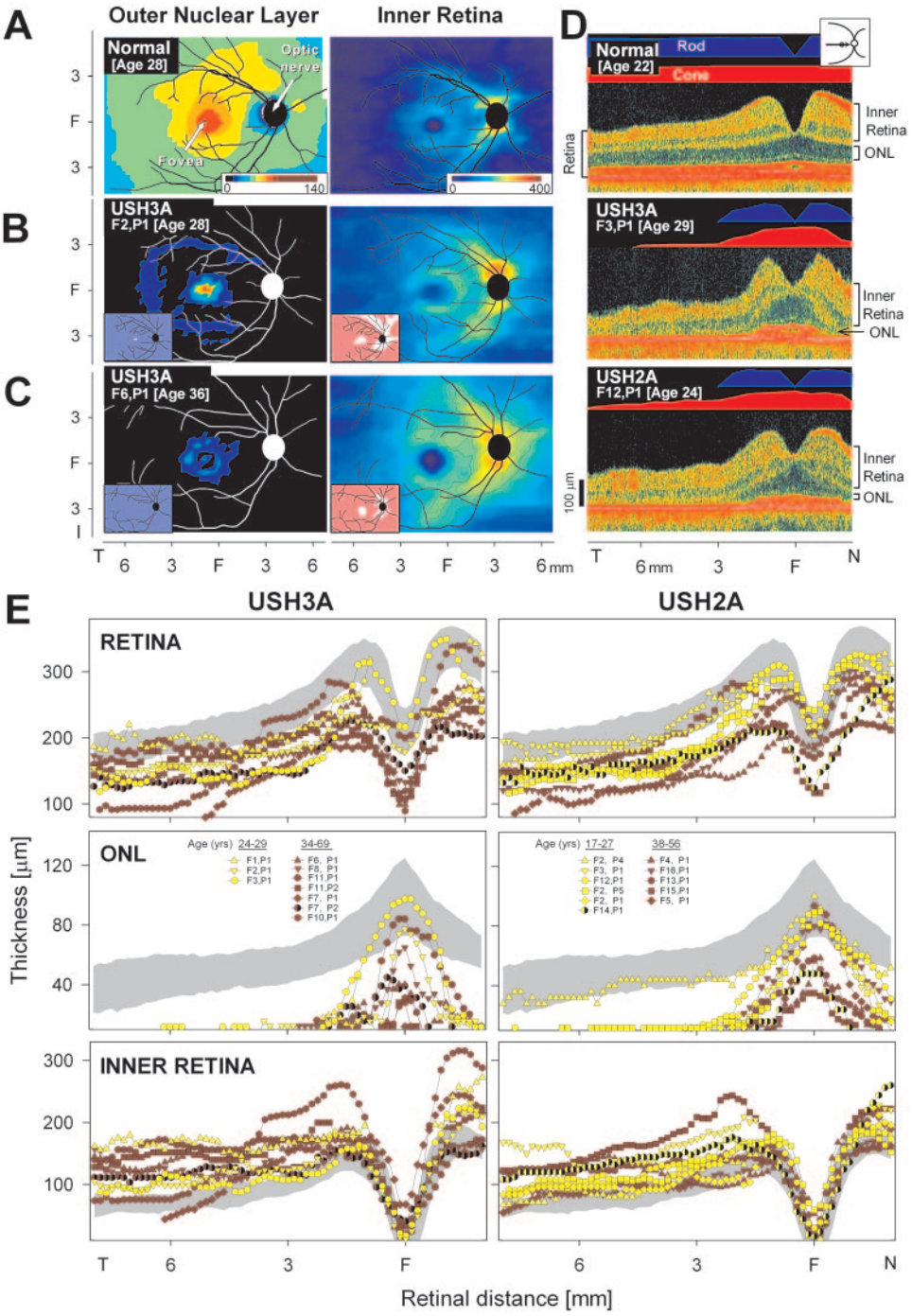

FIGURE 4. Retinal laminar architecture in USH3A and USH2A. (**A–C**) Thickness topography of the ONL and inner retina mapped to a pseudocolor scale (shown beneath normal maps) in a normal subject and two patients with USH3A. *Insets:* thickness difference maps showing region that is abnormally thinned (*blue*), within normal limits (*white*, defined as mean ± 2 SD), or thickened (*pink*), compared to normal. (**D**) Cross-sectional OCT images along the horizontal meridian through the fovea in a normal subject compared with patients with USH3A and USH2A, all in the third decade of life. Brackets defining the ONL and inner retina (*right edge*) and total retinal thickness (*left edge*) are labeled. Bars above cross sections indicate colocalized rod (*blue bar*; dark-adapted, 500 nm) and cone (*red bar*; light-adapted, 600 nm) sensitivity by static perimetry. *Inset:* scan location. (**E**) Thickness of the overall retina (*top*), ONL (*middle*), and inner retina (*bottom*) along the horizontal meridian in patients with USH3A ($n = 10$; *left*) or USH2A ($n = 11$; *right*). Patients are identified by symbols and grouped by age. Measurements are interrupted in regions with, or adjacent to, cystoid changes. *Shaded areas*: normal limits (mean ± 2 SD) for retinal thickness ($n = 27$), ONL ($n = 26$), and inner retina ($n = 14$); age range for all, 5–58 years.

different classes and families, are involved in the process of photoreceptor cell transport.[1,50,51] CLRN1 is currently one of the less well understood USH-associated molecules. Still to be defined are the exact retinal cell and subcompartment localization of CLRN1 and its role in the USH molecular network of proteins. Like most of the other USH genotypes except USH2A,[52] there is no murine model with retinal degeneration for USH3A-*CLRN1*, although work toward that goal is occurring (Flannery J. *IOVS* 2004;45:ARVO E-Abstract 1169).[53]

We sought understanding of the human retinopathy caused by the *CLRN1* mutation by using detailed noninvasive studies of a non-Finnish cohort of patients. *CLRN1* mutations are associated with early-onset rod dysfunction, and rod loss is almost complete in the first two decades of life. Central rod function, however, can be retained at ages when peripheral rod function is no longer detectable. Reduced cone function is measurable in the peripheral field into the third decade of life. Central cone function has a relatively slow decline that extends for decades. Visual dysfunction is accompanied by ONL loss, indicating that the basis of the abnormal function is photoreceptor cell degeneration. It has been suggested that USH3A is involved in photoreceptor synaptic activity.[10,48] At a phenotypic level, there was no evidence of a disturbance of photoreceptor synaptic activity, such as negative electroretinograms or disproportionately preserved ONL in the presence of severe visual abnormalities. USH3A shows reduced retinal thickness in regions with lost ONL and a tendency toward greater retinal thinning in older patients, findings consistent with the histo-

pathology of RP.[54] Inner retinal thickening with loss of normal laminar architecture, attributed to neural and glial remodeling in response to photoreceptor degeneration,[28,31,32,46,47] is also evident in USH3A. Our limited data on NIR-AF topography at relatively advanced disease stages in USH3A support the hypothesis that RPE disease generally parallels photoreceptor degeneration. The ring of parafoveal RPE abnormalities was reminiscent of vulnerability of this retinal region in macular degenerations with various genetic and environmental etiologies.[25,55,56] Better understanding of this feature and the disease sequence will have to await imaging patients at earlier disease stages.

The human retinal phenotype of USH has been discussed as a single disease expression in molecular summaries.[49,50] Is there evidence that the USH interactive network leads to a shared USH retinal phenotype in all genotypes? Evidence has been provided in studies of functional scores of vision from cross-sectional data.[19,57] USH2A and USH1B were reported to be similar.[57] A comparison between Finnish patients with USH3A and Dutch patients with USH1B or USH2A showed similar rates of deterioration in the three molecular subgroups, although some of the data analyses suggested greater severity in USH3A and USH1B than in USH2A.[19]

Our comparisons of USH3A and USH2A retinal phenotypes indicated that the pattern of functional and structural loss in the two molecular subtypes was similar. Peripheral rod function was lost before central rod function; cone function in the periphery was maintained beyond rod loss; and central cone sensitivity and visual acuity persisted longest. Retinal structural abnormalities and the distribution of RPE disease, mainly representing the central retina, were not distinguishable. The findings would be consistent with the hypothesis that dysfunction in the entire USH protein complex could result from an abnormal single component.[51] Differences were noted in the rate of visual decline in USH3A and USH2A. Based on peripheral function measurements, USH3A appeared to be a more rapidly progressive retinal degeneration than did USH2A. The relatively mild early course and subsequent decline in function and structure that we observed in some patients with USH2A (for example, F2,P4; data in Ref. [20]) is reminiscent of the slow time course of disease in the *Ush2a*$^{-/-}$ mouse, the only USH model with retinal degeneration.[52] The upregulated GFAP of Müller cells in the predegenerative state and its persistence throughout the natural history of the murine disease[52] may relate to the thickening of the inner retina in USH2A and the suspected role of Müller cell activation as part of this process.[31,32]

From a clinical perspective, USH diagnostics have become more complex as molecular clarity has increased. Genes associated with classic USH clinical types are now known to cause nonsyndromic deafness and nonsyndromic RP. There are also reports of atypical forms of USH1 with moderate hearing loss and USH2 with progressive hearing loss and some vestibular dysfunction.[17] In the present study, many of the patients with USH3A-*CLRN1* had first received a clinical diagnosis of USH2 or nonsyndromic RP and were later identified when they failed to show mutations in genes other than *CLRN1*. As mutation detection strategies evolve for USH, such as are now occurring for Leber congenital amaurosis,[58] information in addition to clinical diagnosis (e.g., ethnic origins, rate of sensory losses) will help refine and expedite molecular testing and serve the ultimate purpose of developing therapies for these incurable conditions.

Acknowledgments

The authors thank Elaine Smilko, Mary Nguyen, Michelle Doobrajh, and Malgorzata Swider for providing critical help.

References

1. Williams DS. Usher syndrome: animal models, retinal function of Usher proteins, and prospects for gene therapy. *Vision Res.* 2008; 48: 433–441.
2. Fishman GA, Kumar A, Joseph ME, Torok N, Anderson RJ. Usher's syndrome: ophthalmic and neuro-otologic findings suggesting genetic heterogeneity. *Arch Ophthalmol.* 1983;101(9):1367–1374.
3. Kimberling WJ, Moller CG, Davenport SL, et al. Usher syndrome: clinical findings and gene localization studies. *Laryngoscope.* 1989;99(1):66–72.
4. Nuutila A. Dystrophia retinae pigmentosa–dysacusis syndrome (DRD): a study of the Usher- or Hallgren syndrome. *J Genet Hum.* 1970;18(1):57–88.
5. Gorlin RJ, Tilsner TJ, Feinstein S, Duvall AJ 3rd. Usher's syndrome type III. *Arch Otolaryngol.* 1979;105(6):353–354.
6. McDonald JM, Newsome DA, Rintelmann WF. Sensorineural hearing loss in patients with typical retinitis pigmentosa. *Am J Ophthalmol.* 1988;105(2):125–131.
7. Hope CI, Bundey S, Proops D, Fielder AR. Usher syndrome in the city of Birmingham: prevalence and clinical classification. *Br J Ophthalmol.* 1997;81(1):46–53.
8. Joensuu T, Hamalainen R, Lehesjoki AE, de la Chapelle A, Sankila EM. A sequence-ready map of the Usher syndrome type III critical region on chromosome 3q. *Genomics.* 2000;63(3):409–416.
9. Joensuu T, Hamalainen R, Yuan B, et al. Mutations in a novel gene with transmembrane domains underlie Usher syndrome type 3. *Am J Hum Genet.* 2001;69(4):673–684.
10. Adato A, Vreugde S, Joensuu T, et al. USH3A transcripts encode clarin-1, a four-transmembrane-domain protein with a possible role in sensory synapses. *Eur J Hum Genet.* 2002;10(6):339–350.
11. Fields RR, Zhou G, Huang D, et al. Usher syndrome type III: revised genomic structure of the USH3 gene and identification of novel mutations. *Am J Hum Genet.* 2002;71(3):607–617.
12. Aller E, Jaijo T, Oltra S, et al. Mutation screening of USH3 gene (*clarin-1*) in Spanish patients with Usher syndrome: low prevalence and phenotypic variability. *Clin Genet.* 2004;66(6):525–529.
13. Karjalainen S, Pakarinen L, Terasvirta M, Kaariainen H, Vartiainen E. Progressive hearing loss in Usher's syndrome. *Ann Otol Rhinol Laryngol.* 1989;98(11):863–866.
14. Pakarinen L, Karjalainen S, Simola KO, Laippala P, Kaitalo H. Usher's syndrome type 3 in Finland. *Laryngoscope.* 1995;105(6): 613–617.
15. Ness SL, Ben-Yosef T, Bar-Lev A, et al. Genetic homogeneity and phenotypic variability among Ashkenazi Jews with Usher syndrome type III. *J Med Genet.* 2003;40(10):767–772.
16. Pennings RJ, Fields RR, Huygen PL, Deutman AF, Kimberling WJ, Cremers CW. Usher syndrome type III can mimic other types of Usher syndrome. *Ann Otol Rhinol Laryngol.* 2003;112(6):525–530.
17. Cohen M, Bitner-Glindzicz M, Luxon L. The changing face of Usher syndrome: clinical implications. *Int J Audiol.* 2007;46(2):82–93.
18. Pakarinen L, Tuppurainen K, Laippala P, Mantyjarvi M, Puhakka H. The ophthalmological course of Usher syndrome type III. *Int Ophthalmol.* 1996;19(5):307–311.
19. Plantinga RF, Pennings RJ, Huygen PL, et al. Visual impairment in Finnish Usher syndrome type III. *Acta Ophthalmol Scand.* 2006; 84(1):36–41.
20. Schwartz SB, Aleman TS, Cideciyan AV, et al. Disease expression in Usher syndrome caused by VLGR1 gene mutation (USH2C) and comparison with USH2A phenotype. *Invest Ophthalmol Vis Sci.* 2005;46(2):734–743.
21. Jacobson SG, Voigt WJ, Parel JM, et al. Automated light- and dark-adapted perimetry for evaluating retinitis pigmentosa. *Ophthalmology.* 1986;93(12):1604–1611.
22. Jacobson SG, Yagasaki K, Feuer WJ, Román AJ. Interocular asymmetry of visual function in heterozygotes of X-linked retinitis pigmentosa. *Exp Eye Res.* 1989;48(5):679–691.
23. Roman AJ, Schwartz SB, Aleman TS, et al. Quantifying rod photoreceptor-mediated vision in retinal degenerations: dark-adapted thresholds as outcome measures. *Exp Eye Res.* 2005;80(2):259–272.

24. Aleman TS, Cideciyan AV, Volpe NJ, Stevanin G, Brice A, Jacobson SG. Spinocerebellar ataxia type 7(*SCA7*) shows a cone-rod dystrophy phenotype. *Exp Eye Res*. 2002;74(6):737–745.
25. Cideciyan AV, Swider M, Aleman TS, et al. Reduced-illuminance autofluorescence imaging in *ABCA4*-associated retinal degenerations. *J Opt Soc Am A*. 2007;24(5):1457–1467.
26. Weinberger AW, Lappas A, Kirschkamp T, et al. Fundus near infrared fluorescence correlates with fundus near infrared reflectance. *Invest Ophthalmol Vis Sci*. 2006;47(7):3098–3108.
27. Keilhauer CN, Delori FC. Near-infrared autofluorescence imaging of the fundus: visualization of ocular melanin. *Invest Ophthalmol Vis Sci*. 2006;47(8):3556–3564.
28. Cideciyan AV, Aleman TS, Jacobson SG, et al. Centrosomal-ciliary gene CEP290/NPHP6 mutations result in blindness with unexpected sparing of photoreceptors and visual brain: implications for therapy of Leber congenital amaurosis. *Hum Mutat*. 2007;28(11):1074–1083.
29. Huang Y, Cideciyan AV, Papastergiou GI, et al. Relation of optical coherence tomography to microanatomy in normal and rd chickens. *Invest Ophthalmol Vis Sci*. 1998;39(12):2405–2416.
30. Jacobson SG, Cideciyan AV, Aleman TS, et al. Crumbs homolog 1 (*CRB1*) mutations result in a thick human retina with abnormal lamination. *Hum Mol Genet*. 2003;12(9):1073–1078.
31. Jacobson SG, Cideciyan AV, Sumaroka A, et al. Remodeling of the human retina in choroideremia: rab escort protein 1 (*REP-1*) mutations. *Invest Ophthalmol Vis Sci*. 2006;47(9):4113–4120.
32. Aleman TS, Cideciyan AV, Sumaroka A, et al. Inner retinal abnormalities in X-linked retinitis pigmentosa with RPGR mutations. *Invest Ophthalmol Vis Sci*. 2007;48(10):4759–4765.
33. Jacobson SG, Aleman TS, Cideciyan AV, et al. Identifying photoreceptors in blind eyes caused by *RPE65* mutations: prerequisite for human gene therapy success. *Proc Natl Acad Sci USA*. 2005;102(17):6177–6182.
34. Sadeghi M, Cohn ES, Kimberling WJ, Tranebjaerg L, Möller C. Audiological and vestibular features in affected subjects with USH3: a genotype/phenotype correlation. *Int J Audiol*. 2005;44(5):307–316.
35. Berson EL, Sandberg MA, Rosner B, Birch DG, Hanson AH. Natural course of retinitis pigmentosa over a three-year interval. *Am J Ophthalmol*. 1985;99(3):240–251.
36. Massof RW, Dagnelie G, Benzschawel T. First order dynamic of visual field loss in retinitis pigmentosa. *Clin Vis Sci*. 1990;5:1–26.
37. Grover S, Fishman GA, Anderson RJ, Alexander KR, Derlacki DJ. Rate of visual field loss in retinitis pigmentosa. *Ophthalmology*. 1997;104(3):460–465.
38. Birch DG, Anderson JL, Fish GE. Yearly rates of rod and cone functional loss in retinitis pigmentosa and cone-rod dystrophy. *Ophthalmology*. 1999;106(2):258–268.
39. Iannaccone A, Kritchevsky SB, Ciccarelli ML, et al. Kinetics of visual field loss in Usher syndrome type II. *Invest Ophthalmol Vis Sci*. 2004;45(3):784–792.
40. Fishman GA, Bozbeyoglu S, Massof RW, Kimberling W. Natural course of visual field loss in patients with Type 2 Usher syndrome. *Retina*. 2007;27(5):601–608.
41. Flynn MF, Fishman GA, Anderson RJ, Roberts DK. Retrospective longitudinal study of visual acuity change in patients with retinitis pigmentosa. *Retina*. 2001;21(6):639–646.
42. Piazza L, Fishman GA, Farber M, Derlacki D, Anderson RJ. Visual acuity loss in patients with Usher's syndrome. *Arch Ophthalmol*. 1986;104(9):1336–1339.
43. Edwards A, Fishman GA, Anderson RJ, Grover S, Derlacki DJ. Visual acuity and visual field impairment in Usher syndrome. *Arch Ophthalmol*. 1998;116(2):165–168.
44. Tsilou ET, Rubin BI, Caruso RC, et al. Usher syndrome clinical types I and II: could ocular symptoms and signs differentiate between the two types? *Acta Ophthalmol Scand*. 2002;80(2):196–201.
45. Sadeghi AM, Eriksson K, Kimberling WJ, Sjöström A, Möller C. Longterm visual prognosis in Usher syndrome types 1 and 2. *Acta Ophthalmol Scand*. 2006;84(4):537–544.
46. Jacobson SG, Cideciyan AV, Aleman TS, et al. Leber congenital amaurosis caused by *RPGRIP1* mutation shows treatment potential. *Ophthalmology*. 2007;114(5):895–898.
47. Jacobson SG, Sumaroka A, Aleman TS, Cideciyan AV, Danciger M, Farber DB. Evidence for retinal remodelling in retinitis pigmentosa caused by *PDE6B* mutation. *Br J Ophthalmol*. 2007;91(5):699–701.
48. Reiners J, Nagel-Wolfrum K, Jurgens K, Marker T, Wolfrum U. Molecular basis of human Usher syndrome: deciphering the meshes of the Usher protein network provides insights into the pathomechanisms of the Usher disease. *Exp Eye Res*. 2006;83(1):97–119.
49. Kremer H, van Wijk E, Marker T, Wolfrum U, Roepman R. Usher syndrome: molecular links of pathogenesis, proteins and pathways. *Hum Mol Genet*. 2006;15:R262–R270.
50. Maerker T, van Wijk EV, Overlack N, et al. A novel Usher protein network at the periciliary reloading point between molecular transport machineries in vertebrate photoreceptor cells. *Hum Mol Genet.* 2008;17;71–86.
51. Roepman R, Wolfrum U. Protein networks and complexes in photoreceptor cilia. *Subcell Biochem*. 2007;43:209–235.
52. Liu X, Bulgakov OV, Darrow KN, et al. Usherin is required for maintenance of retinal photoreceptors and normal development of cochlear hair cells. *Proc Natl Acad Sci USA*. 2007;104(11):4413–4418.
53. Aarnisalo AA, Pietola L, Joensuu J, et al. Anti-clarin-1 AAV-delivered ribozyme induced apoptosis in the mouse cochlea. *Hear Res*. 2007;230(1–2):9–16.
54. Milam AH, Li ZY, Fariss RN. Histopathology of the human retina in retinitis pigmentosa. *Prog Retin Eye Res*. 1998;17(2):175–205.
55. Weiter JJ, Delori F, Dorey CK. Central sparing in annular macular degeneration. *Am J Ophthalmol*. 1988;106(3):286–292.
56. Cideciyan AV, Swider M, Aleman TS, et al. ABCA4-associated retinal degenerations spare structure and function of the human parapapillary retina. *Invest Ophthalmol Vis Sci*. 2005;46(12):4739–4746.
57. Pennings RJ, Huygen PL, Orten DJ, et al. Evaluation of visual impairment in Usher syndrome 1b and Usher syndrome 2a. *Acta Ophthalmol Scand*. 2004;82(2):131–139.
58. Stone EM. Leber congenital amaurosis: a model for efficient genetic testing of heterogeneous disorders: LXIV Edward Jackson Memorial Lecture. *Am J Ophthalmol.* 2007;144;791–811.